AIP | Journal of Applied Physics

Terahertz gain on intersubband transitions in multilayer delta-doped p - Ge structures

M. V. Dolguikh, A. V. Muravjov, R. E. Peale, M. Klimov, O. A. Kuznetsov, and E. A. Uskova

Citation: Journal of Applied Physics **98**, 023107 (2005); doi: 10.1063/1.1989430
View online: http://dx.doi.org/10.1063/1.1989430
View Table of Contents: http://scitation.aip.org/content/aip/journal/jap/98/2?ver=pdfcov
Published by the AIP Publishing

Articles you may be interested in
Doping in quantum cascade lasers. I. In Al As – In Ga As In P midinfrared devices
J. Appl. Phys. **100**, 043101 (2006); 10.1063/1.2234804

Design and simulation of In Ga As Al As Sb quantum-cascade lasers for short wavelength emission
Appl. Phys. Lett. **87**, 141109 (2005); 10.1063/1.2067701

New p - Ge THz laser spectrometer for the study of solutions: THz absorption spectroscopy of water
Rev. Sci. Instrum. **76**, 063110 (2005); 10.1063/1.1928427

D centers in intracenter Si:P lasers
J. Appl. Phys. **97**, 113708 (2005); 10.1063/1.1922091

Far-infrared laser oscillation from a very small p- Ge crystal under uniaxial stress
Appl. Phys. Lett. **74**, 3432 (1999); 10.1063/1.124118

AIP | Journal of Applied Physics

Journal of Applied Physics is pleased to announce André Anders as its new Editor-in-Chief

[This article is copyrighted as indicated in the article. Reuse of AIP content is subject to the terms at: http://scitation.aip.org/termsconditions. Downloaded to] IP: 132.170.83.1 On: Tue, 08 Jul 2014 15:07:13

HTML ABSTRACT + LINKS

Terahertz gain on intersubband transitions in multilayer delta-doped *p*-Ge structures

M. V. Dolguikh, A. V. Muravjov,[a] and R. E. Peale[b]
Department of Physics, University of Central Florida, Orlando, Florida 32816

M. Klimov
Advanced Materials Processing and Analysis Center, University of Central Florida, Orlando, Florida 32816

O. A. Kuznetsov and E. A. Uskova
Physical-Technical Research Institute, University of Nizhny Novgorod, Nizhny Novgorod 603000, Russia

(Received 24 February 2005; accepted 8 June 2005; published online 28 July 2005)

A far-infrared laser concept based on intersubband transitions of holes in *p*-type periodically delta-doped semiconductor films is studied using numerical Monte Carlo simulation of hot-hole dynamics. The considered device consists of monocrystalline pure Ge layers periodically interleaved with delta-doped layers and operates with vertical hole transport in the presence of an in-plane magnetic field. Population inversion on intersubband transitions arises due to light-hole accumulation in $\mathbf{E}\perp\mathbf{B}$ fields, as in the bulk *p*-Ge laser. However, the considered structure achieves spatial separation of hole accumulation regions from the doped layers, which reduces ionized-impurity and carrier-carrier scattering for the majority of light holes. This allows a remarkable increase of the gain in comparison with bulk *p*-Ge lasers. Population inversion and gain sufficient for laser operation are expected up to 77 K. Test structures grown by chemical-vapor deposition demonstrate feasibility of producing the device with sufficient active thickness to allow quasioptical electrodynamic cavity solutions. © *2005 American Institute of Physics*.
[DOI: 10.1063/1.1989430]

INTRODUCTION

Recent terahertz semiconductor-laser developments include intersubband *p*-Ge lasers,[1] lasers based on optically pumped donors in Si,[2] quantum cascade lasers (QCLs),[3–5] and proposed *p*-type Si/SiGe quantum cascade lasers.[6] All of them suffer from a rapid increase in far-IR lattice absorption with temperature,[7] to offset which requires higher gain and hence higher active carrier concentration, until the population inversion becomes negatively impacted by impurity and carrier-carrier scattering. Terahertz QCLs have achieved continuous-wave (CW) output and operation temperatures above liquid nitrogen via a design with extreme tolerances of quantum-well and barrier thicknesses. This has required growth by molecular-beam epitaxy (MBE), which limits the QCLs active layer thickness to $\sim 10\ \mu$m, requiring complex and lossy cavity solutions.

Among all semiconductor terahertz lasers listed above, only the *p*-Ge laser mechanism for generation of stimulated emission on direct optical intersubband transitions for hot holes has potential for wide tunability (50–140 cm^{-1}). The inverted population grows at certain ratios of the applied crossed electric and magnetic fields at low temperatures, when light holes are accumulated on closed trajectories below the optical-phonon energy, while heavy holes undergo rapid optical-phonon scattering (Fig. 1). The light-hole lifetime, responsible for the inversion population and for the gain, is determined by acoustic-phonon scattering, ionized-impurity scattering, and carrier-carrier interaction. These factors limit *p*-Ge laser operation to liquid-helium temperatures and low carrier concentrations (3×10^{13}–3×10^{14} cm^{-3}). The small signal gain in *p*-Ge lasers usually does not exceed[8] 0.1 cm^{-1}, which is smaller than germanium lattice absorption at 50 K (Fig. 2).[7] This bounds the operating temperature and (because of Joule heating) the duty cycle of bulk *p*-Ge lasers, which usually operate below 20 K and at duty cycles $<\sim 1\%$.

This paper presents a terahertz laser concept based on intersubband transitions of holes under vertical transport in crossed electric **E** and magnetic **B** fields in a planar periodically doped *p*-Ge/Ge structure (Fig. 3). The spacing between

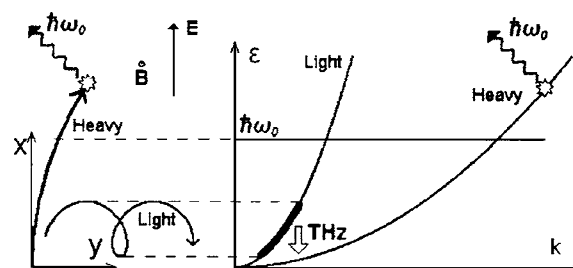

FIG. 1. Mechanism of intersubband population inversion and far-infrared gain for *p*-Ge in crossed electric and magnetic fields. The left part of the diagram shows light- and heavy-hole trajectories in coordinate space. The right part of the diagram shows light- and heavy-hole subband energies vs momentum wave vector together with trajectories and vertical intersubband radiative transitions. The optical-phonon scattering threshold is indicated by the horizontal line $\hbar\omega_0$ in both parts, and optical-phonon emission by heavy holes is indicated by the wavy arrows.

[a]On leave from Institute of the Physics of Microstructures, RAS, Nizhny Novgorod, Russia.
[b]Electronic mail: rep@physics.ucf.edu

[This article is copyrighted as indicated in the article. Reuse of AIP content is subject to the terms at: http://scitation.aip.org/termsconditions. Downloaded to] IP: 132.170.83.1 On: Tue, 08 Jul 2014 15:07:13

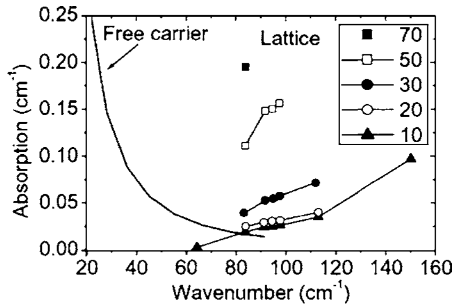

FIG. 2. Far-infrared absorption in Ge. Temperature-dependent lattice absorption (see Ref. 7) is plotted as connected symbols, with temperature in K indicated in the legend. The free-carrier absorption for hole concentration of 2×10^{14} cm^{-3} calculated for typical bulk p-Ge distribution functions is plotted as a solid curve.

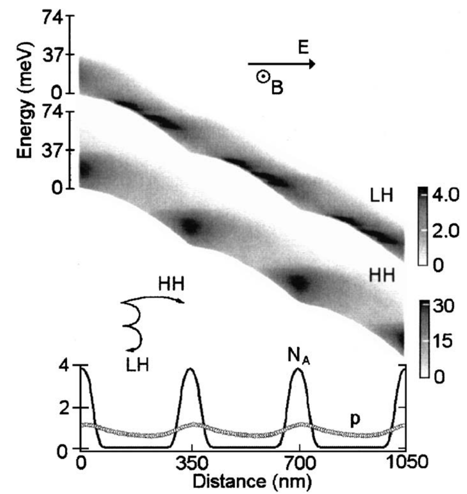

FIG. 3. Spatial separation of carriers and intersubband mechanism of terahertz amplification for delta-doped multilayer Ge structures in $\mathbf{E}\times\mathbf{B}$ fields. The dark areas represent high concentrations of light holes (upper band) and heavy holes (lower band). The shading scale is in units of 10^{12} cm^{-3} meV^{-1}. The spatial dependence of the zero-energy edge of the hole distribution reflects the self-consistent potential profile. Acceptor concentration profile N_A and total hole concentration p across the structure are plotted in units of 10^{15} cm^{-3}. The simulation parameters were $E=1.5$ kV/cm, $B=1.15$ T, $T=10$ K, and $N_{\text{av}}=8\times10^{14}$ cm^{-3}. Schematic light- and heavy-hole cyclotron trajectories are drawn to scale in coordinate space.

doped layers is considered to be 300–400 nm, which is wider than the average light-hole Larmor radius at 1–3 T applied B fields. The design achieves spatial separation of hole accumulation regions from the doped layers, which reduces ionized-impurity and carrier-carrier scatterings for the majority of light holes, allowing significant increase of the total carrier concentration while maintaining sufficient light-hole lifetime. The resulting increase in gain over the bulk p-Ge laser promises to raise maximum operation temperatures to 77 K. At the same time the proposed laser retains the most attractive feature of the hot-hole intersubband mechanism, which is its wide tunability over the spectral range of 2–4 THz. Preliminary investigation of this structure was reported in Ref. 9.

THEORETICAL METHODS

Hole dynamics, hole distribution functions, and the gain on direct optical light-to-heavy hole transitions are calculated by the Monte Carlo simulation method using classical motion equations and hole scattering probabilities.[10,11] A classical approach to the hole dispersion law and equations of motion is justified here by the moderate magnetic fields and the absence of heteroboundaries. At 1 T magnetic field, the quantization energy of Landau levels is $\Delta E_B=2.7$ and 0.33 meV for light and heavy holes, respectively. Hence, the Landau quantization energy of light holes is sufficiently less than the average hole energy $E_{\text{av}}\sim15$ meV to neglect quantum effects. Analysis of Landau quantization and other quantum effects in crossed electric and magnetic fields for the p-Ge lasers is reported in Refs. 12 and 13. We can neglect quantum confinement effects because the considered structure has no heteroboundaries, only delta-doped layers.

Time- or ensemble-averaged momentum and position yield the hole distribution functions $f_{l,h}(\mathbf{k},\mathbf{r})$ [subband (l,h), wave vector $\mathbf{k}$ and coordinate $\mathbf{r}$]. The distribution functions were considered uniform in the horizontal planes according to the geometry of the problem. Two valence subbands (light and heavy holes) with isotropic and parabolic dispersion laws are considered: $E_{l,h}=\hbar^2k^2/2m_{l,h}$. The isotropic approach is justified by the relatively small warping of the germanium valence band. The standard Rees rejection technique chooses among the scattering processes.[10] The rate of each scattering process is given by a temperature-dependent analytic expression. Optical-phonon scattering is treated in a deformation potential approximation.[14,15] Acoustic-phonon scattering is simplified according to Ref. 16. Inelasticity for acoustic-phonon scattering is included.[17] The Brooks-Herring model[18] with the inverse Debye screening length and the Yukawa potential was used for ionized-impurity scattering.

An accurate treatment of carrier-carrier scattering is essential for our simulations because high average carrier concentrations are a goal. Traditionally, carrier-carrier scattering was taken into account by doubling the quantity of scattering centers compared with the acceptor concentration.[8,17] In contrast, angular-dependent four-dimensional (three-dimensional (3D) momentum space and one-dimensional (1D) vertical coordinate) distribution functions of light and heavy holes are used here to calculate carrier-carrier scattering probabilities and scattering angles.[19] For the Coulomb interaction potential with a Yukawa-type screening, the transition rate for the $\mathbf{k}_1+\mathbf{k}_2\Rightarrow\mathbf{k}_3+\mathbf{k}_4$ process can be calculated as

$$P_{1,2\to3,4}\cong\frac{2\pi}{\hbar}\left|\langle\Psi_{3,4}|\frac{e^2\exp(-\beta|\mathbf{r}_1-\mathbf{r}_2|)}{4\pi\varepsilon\varepsilon_0|\mathbf{r}_1-\mathbf{r}_2|}|\Psi_{1,2}\rangle\right|^2\times\delta(E_1+E_2-E_3-E_4),\qquad(1)$$

where $\mathbf{k}_i$ is the hole wave vector, $\hbar$ is the Planck constant, e is the electron charge, β is the screening parameter, ε is the relative dielectric constant, ε_0 is the permittivity of free space, and E_i is the hole kinetic energy. The two-particle states were taken as products of single hole wave functions in the ith state, given by

[This article is copyrighted as indicated in the article. Reuse of AIP content is subject to the terms at: http://scitation.aip.org/termsconditions. Downloaded to] IP: 132.170.83.1 On: Tue, 08 Jul 2014 15:07:13

$$\psi_i(\mathbf{k}_i,\mathbf{r}) = \exp(i\mathbf{k}_i\mathbf{r}) \sum_{m_J=\pm 3/2,\pm 1/2} c^{3/2}_{m_J,i}(\mathbf{k}_i)\psi^{3/2}_{m_J}. \quad (2)$$

The $\psi^{3/2}_{m_J}$ are basis functions in the Luttinger-Kohn representation.[14,20] The coefficients $c^{3/2}_{m_J}(\mathbf{k})$ are known functions of the direction of hole motion.[14] There are two sets of four coefficients corresponding to light holes and two sets corresponding to heavy holes. It is the angular dependence of these coefficients that gives an angle dependence to the probabilities in Eq. (1). The total single hole transition probability mediated by hole-hole interaction is

$$P(k_1) \propto \int P_{1,2\to 3,4}(\mathbf{k}_1,\mathbf{k}_2,\mathbf{k}_3,\mathbf{k}_4,v_1,v_2,v_3,v_4) \times f_{v_1}(\mathbf{k}_1)f_{v_2}(\mathbf{k}_2)d\Omega_1 d\mathbf{k}_2 d\mathbf{k}_3 d\mathbf{k}_4, \quad (3)$$

where f_v is the hole distribution function in vth subband and $d\Omega_1$ is the solid angle element for the direction of incidence of the first hole. A similar formula is used for ionized-impurity scattering (without the factors and distribution functions for the second hole). These integrations are performed using the distribution functions calculated from the Monte Carlo simulations.

The Monte Carlo code was specially written to allow spatially varying impurity and hole-hole scattering probabilities for simulation of carrier dynamics with stratified parameters (Fig. 3). In order to solve the problem self-consistently, taking into account internal electric fields caused by charge separation, infinite-charged planes are assumed, which is well justified by the structure geometry. The redistribution of space charge, which we find to become important at average concentrations above 10^{14} cm^{-3}, is included as an additional "internal" electric field E_{int}. Iteration determines the self-consistent solution of the Poisson equation and thereof the spatial carrier distribution and potential profile. The total electric field across the structure is given by $E=-\partial\varphi/\partial x = E_{\text{int}}+E_{\text{appl}}$, where E_{appl} is the applied external field and φ is the electric potential. For any distribution of holes $p(x)$ and negatively charged acceptor impurity centers $N(x)$, the internal electric field along the period of the structure d is

$$E_{\text{int}}(x) = E_0 + \frac{e}{\varepsilon\varepsilon_0}\int_0^x [p(x) - N(x)]dx. \quad (4)$$

Due to periodicity and total neutrality of the crystal,

$$E_{\text{int}}(x) = E_{\text{int}}(x+d), \quad (5)$$

and

$$\int_0^d E_{\text{int}}(x)dx = 0. \quad (6)$$

For these particular simulations we assumed zero compensation, so that all introduced doping centers are shallow acceptors.

The small signal gain is calculated as the difference between the gain on direct intersubband (light to heavy hole) transitions and free-carrier absorption assisted by phonons and ionized impurities.[17,21] The intersubband gain is given by

$$\alpha_{lh}(\mathbf{r},hv) = \frac{\pi e^2\hbar}{m_e\varepsilon_0\varepsilon^{1/2}c}\int \frac{d\mathbf{k}}{(2\pi)^3}|\zeta_{lh}(\mathbf{k})| \times [f_l(\mathbf{k},\mathbf{r}) - f_h(\mathbf{k},\mathbf{r})]\delta[\varepsilon_l(\mathbf{k}) - \varepsilon_h(\mathbf{k}) - hv], \quad (7)$$

where the distribution functions $f_{l,h}(k,r)$ for light and heavy holes are simulation outputs, $\varepsilon_{l,h}(k)$ are the hole energies, m_e is the electron mass, ε is the relative dielectric constant, c is the speed of light in vacuum, and ζ_{lh} is the unpolarized oscillator strength.[22] The light- and heavy-hole distribution functions are normalized to the total local hole concentration,

$$p(\mathbf{r}) = \int [f_l(\mathbf{k},\mathbf{r}) + f_h(\mathbf{k},\mathbf{r})]\frac{2d\mathbf{k}}{(2\pi)^3}. \quad (8)$$

Analysis of various scattering-mechanism contributions to free-carrier absorption is given in Ref. 21. Up to liquid-nitrogen temperatures and impurity concentrations of $\sim 10^{15}-10^{16}$ cm^{-3}, the main contribution comes from the optical-phonon emission by heavy holes.

CALCULATION RESULTS

Applied fields and the period of the structure are chosen so that the average light-hole orbits are smaller than the doping period while heavy holes suffer strong impurity scattering at the doped layers. Figure 3 presents the calculated light- and heavy-hole energy distributions in the multilayer delta-doped Ge structure as functions of space coordinate and energy. The calculated energy-spatial distribution of light (upper band) and heavy (lower band) holes is presented in units of 10^{12} cm^{-3} meV^{-1}. The spatial dependence of the zero-energy edge of the hole distributions reflects the self-consistent potential profile. The spatial separation of light and heavy holes across the structure period for transport in $\mathbf{E}\times\mathbf{B}$ fields is revealed in the density map of the distributions shown in Fig. 3. Heavy holes are preferably concentrated near the doped layers and scatter on optical phonons (37 meV) and ionized impurities. Meanwhile, light holes accumulate below the optical-phonon energy without optical-phonon scattering. Moreover, their distribution function is maximum in undoped regions, where ionized-impurity and carrier-carrier scattering rates are suppressed.

Although impurity scattering has been eliminated from the light-hole accumulation regions of our device, hole-hole scattering remains, and this is the primary scattering mechanism responsible for the light-hole lifetime and thus for the final performance of the device. The total light-to-heavy intersubband scattering rates on carriers and impurities [Eq. (3)] are compared in Fig. 4 as a function of the scattering center concentration for two different values of light-hole kinetic energy. (These are nonradiative transitions that depopulate the upper laser level.) Figure 4 reveals that hole-hole intersubband scattering rates are consistently lower than those for ionized-impurity scattering. Thus, the elimination of impurity scattering from light-hole accumulation regions and the comparatively ineffective light-to-heavy band relaxation caused by hole-hole interaction permit more than a factor of 2 increase in carrier density in comparison with the

[This article is copyrighted as indicated in the article. Reuse of AIP content is subject to the terms at: http://scitation.aip.org/termsconditions. Downloaded to] IP: 132.170.83.1 On: Tue, 08 Jul 2014 15:07:13

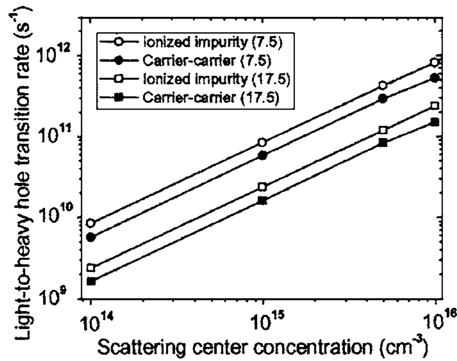

FIG. 4. Carrier-carrier and ionized-impurity scattering rates for the light-to-heavy hole nonradiative intersubband transition averaged over typical p-Ge laser light- and heavy-hole distribution functions ($E=1.5$ kV/cm, $B=1.1$ T, and $T=10$ K) vs scattering center concentration. The values in the legend indicate the initial light-hole kinetic energy in meV.

bulk p-Ge laser. The suppressed heavy-hole concentration in these undoped regions, revealed in Fig. 3, favors even further concentration increase and a corresponding increase in gain.

Figures 5 and 6 present the calculated gain spectra for the same concentration but two different applied field conditions. The average carrier concentration chosen is already about a factor of 10 larger than usual for bulk p-Ge lasers. Gain is plotted as a function of the optical transition wave number and vertical distance within the structure for two structure periods. Each figure shows results for three different temperatures: 10, 50, and 77 K. A dark line indicates the intersection of the gain surfaces with the horizontal plane of zero gain. The gain remains positive in the undoped regions of the structure up to lattice temperatures of 77 K. Comparison of Figs. 5 and 6 shows that higher applied fields are required to support the nonequilibrium distribution needed for positive spatially averaged gain at higher lattice temperatures because of the thermalization of holes on phonons.

Spatially averaged gain spectra at 10 and 50 K for the two applied field conditions of Figs. 5 and 6 are presented in Fig. 7 together with lattice absorption spectra.[7] Gain values of $0.5-0.7$ cm^{-1} in the spectral range of $60-140$ cm^{-1} exceed the maximum lattice absorption at 10 K by a factor of 5–7. At $T=50$ K peak gain ($0.15-0.2$ cm^{-1}) still exceeds absorption for the higher fields. Additional calculations at even higher fields ($E\sim 3$ kV/cm and $B\sim 3$ T), shorter period ($d \sim 200$ nm), and higher concentrations ($N_{\rm av}\sim 1-2 \times 10^{15}$ cm^{-3}) suggest sufficient gain for 77 K laser operation. Note that at these magnetic fields and structure periods, the classical approach in the simulations becomes limited due to Landau quantization considerations. However, as was shown previously,[23] the spectrally smooth small signal gain calculated in the classical approach is in good agreement with the spectrally averaged gain calculated in a quantum approach.

Figure 8 presents the dependence of the spatially averaged gain at different wave numbers as a function of the structure period for a fixed fractional thickness of the doped layers ($0.1d$). The optimum period is found to be in the range of $300-500$ nm, depending on the generated optical transition wave number. The calculated gain for bulk p-Ge with

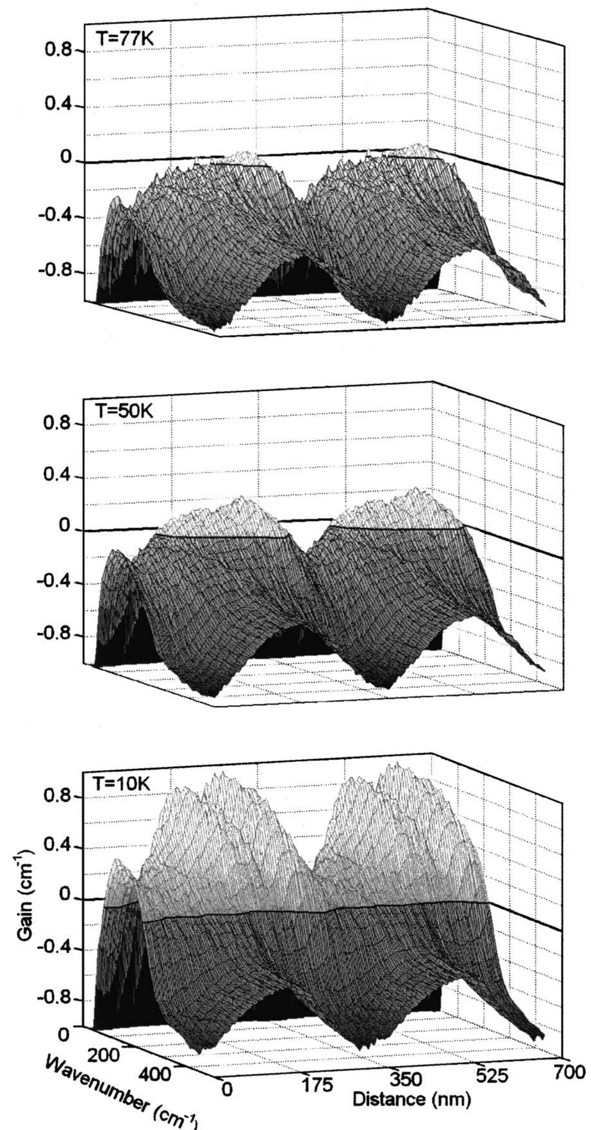

FIG. 5. Spatial-spectral gain distribution across two structure periods with $N_{\rm av}=8\times 10^{14}$ cm^{-3} for low applied fields ($E=1.5$ kV/cm and $B=1.15$ T). Simulation temperatures are indicated.

the same applied fields and concentration is also presented for comparison. The gain for the structure tends toward the bulk values as the period goes to zero.

Figure 9 shows the dependence of the gain spectrum on the electric field at a fixed magnetic field. The optimal field ratio is found to be about 1.5 kV/(cm T) at B=1.5 T, which is very close to the optimal field ratio in the bulk p-Ge laser.[8] Note also the shift of the peak toward a higher wave number as the electric field is increased, which occurs also in bulk p-Ge lasers.

GROWTH FEASIBILITY

For initial experimental feasibility study, Ge:B delta-doped structures were grown by chemical-vapor deposition (CVD). The CVD method is based on hydride epitaxy, in which Ge layers are formed by the pyrolysis of germane (GeH_4) gas on heated substrates. The setup for gas hydride epitaxy of pure and doped Ge layers was developed at the

[This article is copyrighted as indicated in the article. Reuse of AIP content is subject to the terms at: http://scitation.aip.org/termsconditions. Downloaded to] IP: 132.170.83.1 On: Tue, 08 Jul 2014 15:07:13

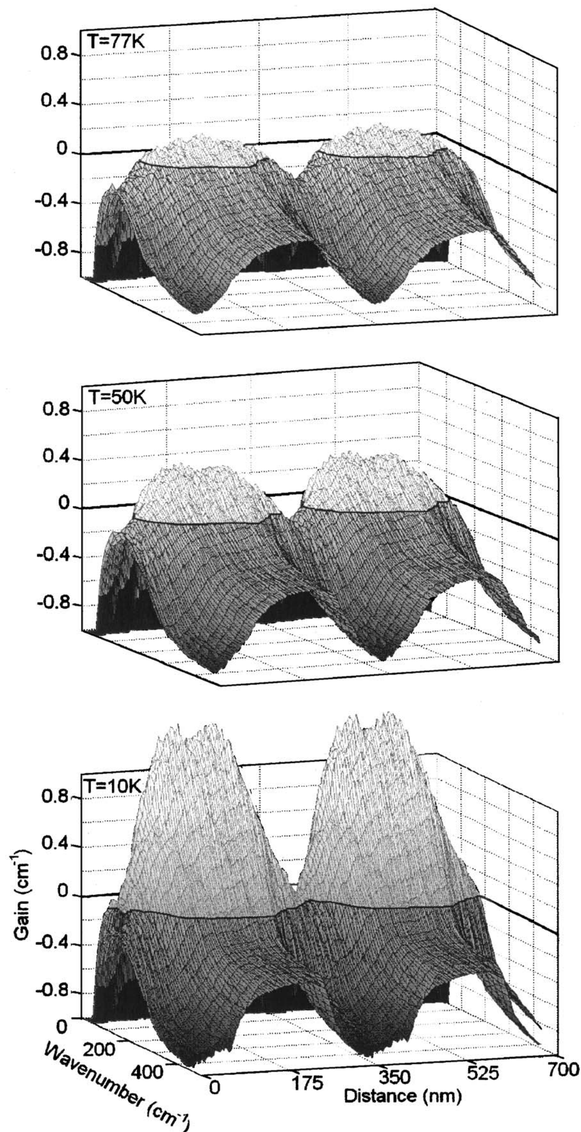

FIG. 6. Spatial-spectral gain distribution across two structure periods with $N_{av}=8\times10^{14}$ cm^{-3} for high applied fields ($E=2.5$ kV/cm and $B=2$ T). Simulation temperatures are indicated.

Physico-Technical Research Institute at Nizhny Novgorod State University. It features a water-cooled horizontal-type reactor with a straight-channel carbon heater. A mixture of hydrides and hydrogen is fed into one side of the reactor and exhaust gases are removed from the other side. The substrate temperature is controlled by an electro-optical transformer for a temperature range of 500–850 °C. Automatic regulation of gas flow by personal computer (PC)-controlled electromagnetic valves allows the growth of multilayer structures with complex concentration profiles. For the layer thickness measurements, a microanalytical balance with a 0.01–0.1-mg accuracy is used, which gives thickness accuracy of 2–20 nm for 35-mm substrates. Germane, like all other hydrides, is a gas, which at normal conditions is far from saturation. The secondary product of thermal depletion is H_2, which is the same as the carrier gas used. The germane used is highly purified, such that the crystals grown from it should have a concentration of electronically active impurities below 10^{13} cm^{-3}. For boron acceptor doping, another

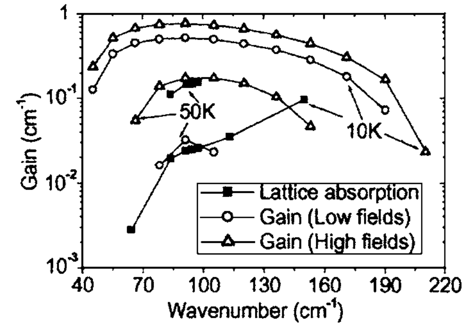

FIG. 7. Spatially averaged calculated THz gain spectra (open symbols) with $N_{av}=8\times10^{14}$ cm^{-3} for low ($E=1.5$ kV/cm and $B=1.15$ T) and high ($E=2.5$ kV/cm and $B=2$ T) applied fields at two different lattice temperatures. The experimental lattice absorption spectra (see Ref. 7) in Ge at $T=10$ and 50 K are plotted as solid symbols.

hydride B_2H_6 is used. Relatively low growth temperatures in the range of 600–750 °C prevent significant diffusion of the doping concentration profiles. The growth speed of 0.5 μm/min is very high compared with ~1 μm/h for MBE.

Several selectively doped Ge:B test structures of different thicknesses (11–32 μm) have been grown, although the peak concentration of these initial test structures was higher than the optimal value required for gain. Figure 10 shows the secondary-ion-mass spectrometer (SIMS) data taken from one of the test structures, which consist of 35 periods with a total thickness of 14 μm. The linear SIMS spectrum in Fig. 11 shows more clearly the achieved doping profile. Diffusion of acceptors from doped layers during CVD growth is observed to be insignificant.

According to our calculations, the pure Ge regions require an ionized-impurity concentration below 3–5 $\times10^{13}$ cm^{-3}, since the amplification cross section starts to decrease at higher concentrations due to ionized-impurity scattering.[9] That this is achievable by CVD was verified by electron-beam-induced current (EBIC) measurements,[24] which determine the minority-carrier diffusion length, a function of impurity concentration. The diffusion length for an undoped CVD Ge sample was compared with a calibration curve obtained using bulk Ge standards, and the net impurity concentration was found to be about 10^{13} cm^{-3}. High-resolution transmission electron micrographs revealed

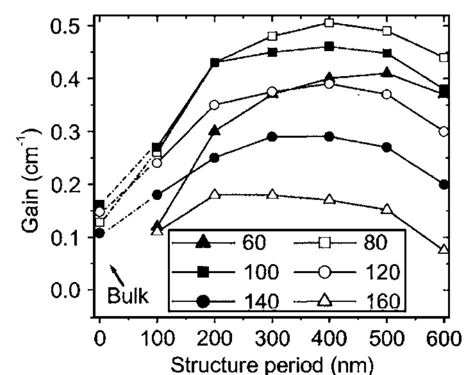

FIG. 8. Spatially averaged gain vs structure period. The legend gives the transition wave number for each curve in units of cm^{-1}. $E=2.25$ kV/cm and $B=1.5$ T, $T=10$ K, and $N_{av}=5\times10^{14}$ cm^{-3}.

[This article is copyrighted as indicated in the article. Reuse of AIP content is subject to the terms at: http://scitation.aip.org/termsconditions. Downloaded to] IP: 132.170.83.1 On: Tue, 08 Jul 2014 15:07:13

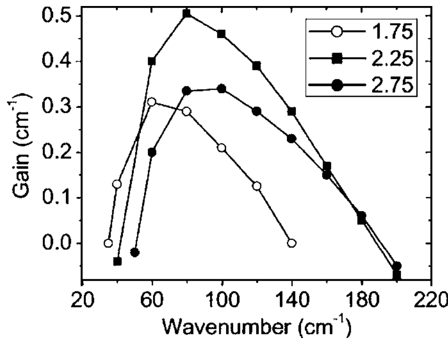

FIG. 9. Spatially averaged gain spectra for different electric fields at fixed magnetic field for the structure with a period of 400 nm, $N_{av}=5\times10^{14}$ cm^{-3}, $T=10$ K, and $B=1.5$ T. The legend gives the electric field value for each curve in kV/cm.

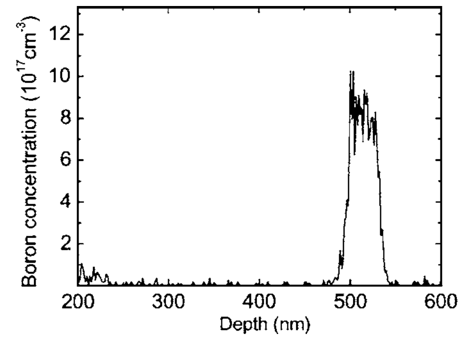

FIG. 11. Linear SIMS spectrum of the first period of the structure to determine the impurity diffusion profile.

no evidence of defects or dislocations at the interface between CVD Ge film and Ge substrate.[25,26] Hence, the growth test demonstrated feasibility of our setup to grow the considered delta-doped Ge structures to relatively high thicknesses without negative effect on the crystal or structure quality.

DISCUSSION

At 10 K, the calculated small signal gain in the proposed delta-doped thin-film *p*-Ge laser design was found to be three to four times higher (Fig. 8) at the same applied fields than that calculated for bulk *p*-Ge lasers at the same average carrier concentration. However, the elimination of ionized-impurity scattering and the reduction of heavy-hole scattering in the undoped accumulation regions allow considerable increase in the average carrier concentration for the structure over bulk, with a corresponding increase in the gain. Higher gain permits smaller, planar active volume (which facilitates cooling) and lower electric-field threshold (which lowers Joule heating). This leads to a higher achievable duty cycle and perhaps to continuous wave operation. Positive total gain at 50–77 K will permit operation in a compact Stirling refrigerator or in liquid nitrogen.

The simplicity of the considered structure allows fast growth by chemical-vapor deposition,[26] which can achieve a significantly thicker active region compared with a MBE-grown QCL. In favor of increased thickness for homoepitaxial structures is the absence of heterointerfaces and stress between layers. In support of these assertions we demonstrated experimentally that CVD can produce thick (>30 μm) multilayer delta-doped Ge structures with sufficiently sharp doping profiles, sufficiently pure undoped regions, and high crystal quality. This allows quasioptical electrodynamic cavity design with remarkably reduced losses compared with double-metal or plasma waveguides that have been used for the comparatively thin QCL THz lasers.[3–5] Small electrodynamic losses will allow the delta-doped multilayer Ge laser to operate with THz gain levels of 0.4–0.5 cm^{-1}. The absence of confinement quantization of the energy spectrum will permit wide tunability over the very broad spectral range of 60–140 cm^{-1} (Fig. 7).

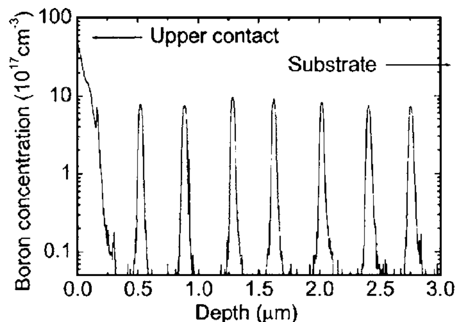

FIG. 10. Semilogarithmic SIMS spectrum of boron for the first seven periods of a CVD-grown 35 period *p*-Ge/Ge structure. The intentional high boron concentration on the surface is intended as a contact layer.

ACKNOWLEDGMENT

This work was supported in part by AFOSR Contract Nos. F49620-02-C-0025 and F49620-02-C-0027.

[1] E. Bründermann, in *Long Wavelength Infrared Semiconductor Lasers*, edited by H. K. Choi (Wiley, Hoboken, New Jersey, 2004), pp. 279–343.
[2] S. G. Pavlov, R. Kh. Zhukavin, E. E. Orlova, V. N. Shastin, A. V. Kirsanov, H.-W. Huebers, K. Auien, and H. Riemann, Phys. Rev. Lett. **84**, 5220 (2000).
[3] B. S. Williams, H. Callebaut, S. Kumar, Q. Hu, and J. L. Reno, Appl. Phys. Lett. **82**, 1015 (2003).
[4] R. Kohler *et al.*, Nature (London) **417**, 156 (2002).
[5] M. Rochat, L. Ajili, H. Willenberg, J. Faist, H. Beere, G. Davies, E. Linfield, and D. Ritchie, Appl. Phys. Lett. **81**, 1381 (2002).
[6] R. Bates *et al.*, Appl. Phys. Lett. **83**, 4092 (2003).
[7] R. Brazis and F. Keilmann, Solid State Commun. **70**, 1109 (1989).
[8] V. N. Shastin, Opt. Quantum Electron. **23**, S111 (1991).
[9] M. V. Dolguikh, A. V. Muravjov, and R. E. Peale, Proc. SPIE **5365**, 184 (2004).
[10] C. Jacoboni and L. Reggiani, Rev. Mod. Phys. **55**, 645 (1983).
[11] C. Jacoboni, R. Brunetti, and P. Bordone, in *Theory of Transport Properties of Semiconductor Nanostructures*, edited by E. Scholl (Chapman and Hall, London, 1998), p. 59.
[12] Yu. Mityagin, V. N. Murzin, and S. A. Stoklitsky, Opt. Quantum Electron. **23**, S287 (1991).
[13] A. V. Murav'jov and V. N. Shastin, Opt. Quantum Electron. **23**, S313 (1991).
[14] G. L. Bir and G. E. Pikus, *Symmetry and Strain-induced Effects in Semiconductors* (Wiley, New York, 1974).
[15] P. Lawaetz, Phys. Rev. **174**, 867 (1968).
[16] J. D. Wiley, Phys. Rev. B **4**, 2485 (1970).
[17] E. V. Starikov and P. N. Shiktorov, Opt. Quantum Electron. **23**, S177 (1991).
[18] B. K. Ridley, J. Phys. C **10**, 1589 (1977).
[19] A. V. Muravjov, M. V. Dolguikh, R. E. Peale, O. A. Kuznetsov, and E. A. Uskova, Proc. SPIE **5727**, 44 (2005).
[20] J. M. Luttinger and W. Kohn, Phys. Rev. **97**, 869 (1955).
[21] Yu. K. Pozhela, E. V. Starikov, and P. N. Shiktorov, Phys. Status Solidi B **128**, 653 (1985).

[This article is copyrighted as indicated in the article. Reuse of AIP content is subject to the terms at: http://scitation.aip.org/termsconditions. Downloaded to] IP: 132.170.83.1 On: Tue, 08 Jul 2014 15:07:13

[22]Yu. T. Rebane, Sov. Phys. Solid State **25**, 1094 (1983).
[23]A. V. Murav'ev, Yu. N. Nozdrin, and V. N. Shastin, JETP Lett. **43**, 449 (1986).
[24]Zaubertek/UCF, AFOSR Contract No. F49620-02-C-0025 final report, 2003 (unpublished).
[25]R. Van Fleet, private communication.
[26]M. V. Dolguikh, A. V. Muravjov, and R. E. Peale, Proc. SPIE **5411**, 207 (2004).

[This article is copyrighted as indicated in the article. Reuse of AIP content is subject to the terms at: http://scitation.aip.org/termsconditions. Downloaded to] IP: 132.170.83.1 On: Tue, 08 Jul 2014 15:07:13